

Acoustic Modal Testing of Bicycle Rims

Matthew Ford · Patrick Peng · Oluwaseyi Balogun

Received: 1 September 2017 / Accepted: 7 February 2018

Abstract The stiffness, strength, and safety of a bicycle wheel depend critically on the stiffness of its rim. However, the complicated cross-sections of modern bicycle rims make estimation of the stiffness by geometric methods very difficult. We have measured the radial bending stiffness and lateral-torsional stiffness of bicycle rims by experimental modal analysis using a smartphone microphone. Our acoustic method is fast, cheap, and non-destructive, and estimates the radial bending stiffness, EI_{11} , to within 8% and the torsional stiffness, GJ , to within 11% as compared with a direct mechanical test. The acoustic method also provides a direct measurement of the coupled lateral-torsional effective stiffness, which is necessary for calculating many useful properties of bicycle wheels such as stiffness, buckling tension, and the influence of spoke tensioning. For a complete bicycle wheel, the lateral stiffness can be determined by a superposition of equivalent springs for each mode in series, where each mode stiffness contains a rim stiffness and spoke stiffness combined in parallel. We give example calculations on two realistic bicycle wheels using our experimentally derived rim properties to show how stiff spokes can compensate for a flexible rim, while a very stiff rim doesn't necessarily result in a stiff wheel.

Keywords experimental modal analysis · acoustics · bicycle wheel · structural characterization · smartphone applications

M. Ford · P. Peng · O. Balogun
Dept. of Mechanical Engineering, Northwestern University
2145 Sheridan Road, Evanston, IL 60208

M. Ford
Tel: +1 847-491-3054
E-mail: mford@u.northwestern.edu

1 Introduction

The ubiquity, connectivity, and computational power of smartphones have inspired applications in non-destructive evaluation (NDE) and structural health monitoring (SHM). The built-in accelerometer has been used to identify natural modes of buildings and bridges [1], measure inclination angles [2], and detect and quantify seismic events [3]. Smartphone accelerometers generally have a maximum frequency of 50-100 Hz, and thus are limited to measuring seismic activity or natural modes of large structures.

The microphone picks up where the accelerometer leaves off: the one used in this study has a relatively flat frequency response above 100 Hz. Although the microphone has received limited attention for NDE applications, smartphone microphones have been used for close-range sonar measurements [2], detecting roller bearing failures [4], and measuring bicycle spoke tension [5]. Other potential applications in the audible range include concrete bridge deck inspections, which often rely on the operator's trained ear to detect anomalies, and rapid inspection of automotive assemblies during manufacturing. In this paper we present a novel application using a smartphone microphone for quantitative, model-based NDE of bicycle rims.

The stiffness [6], truing response [7], and maximum spoke tension [8] of a bicycle wheel depend partly on the stiffness of the rim in bending and torsion. Rim cross-sections typically have complicated shapes with multiple open and closed regions and the exact shape and wall thickness cannot be easily determined without a destructive test. Furthermore, the spoke holes reduce the effective bending stiffness over relevant length scales in a complex manner [9]. Therefore, it is desirable to

obtain the rim section properties experimentally and with minimal assumptions or computation.

Pippard and Francis [6, 10] undertook the first quantitative experimental investigations of the stiffness of spoked wheels and compared their results with an analytical solution. For the special case of radial loads, they determined the in-plane bending stiffness of bare rims by diametral extension. The rims that they tested were cut from a steel plate and all had rectangular cross-sections of varying aspect ratio and did not resemble the complicated cross-sections of modern rims. Due to the difficulty of determining the out-of-plane bending stiffness and torsional stiffness of a circular beam, their investigation of lateral deformations was limited to theory alone. Burgoyne and Dilmaghalian [11] performed experiments on bicycle wheels and compared their results with Pippard's theory. They calculated the radial bending stiffness of the rim from geometric analysis of its cross-section, but their study was limited to radial loads. Gavin [9] noted that the out-of-plane bending stiffness and torsional stiffness are coupled in curved beams and require at least two independent measurements to determine. He performed out-of-plane deflection tests while clamping the rim at two points with various arc lengths. This method requires rigid clamps and neglects warping of the cross-section.

Experimental Modal Analysis (EMA) [12] is a technique for inspecting structures to predict the dynamic response, assess the quality of a manufactured product, or monitor the health of an existing structure [13]. In one variant of EMA, the structure is impulsively excited and then monitored using one or more accelerometers or contact transducers. With enough transducers, both the natural frequencies and mode shapes may be estimated. If spatial information is not required and the modes of interest have sufficiently high acoustic coupling in air, a microphone may be used to obtain a spectrum, allowing for non-contact measurement.

We have developed a method for measuring the stiffness of bicycle rims for both in-plane and out-of-plane loads using quantitative model-based EMA. Our method is fast, non-destructive, and can be performed with only simple household tools including a weight scale, a piece of string, and a smartphone. Together with knowledge of the spoke geometry and material properties, our test can be used to determine the bicycle wheel's radial stiffness, lateral stiffness, and maximum safe tension before buckling. For the purposes of validating the technique we also compare the calculated stiffness from the acoustic test with quasistatic load-displacement tests in both the radial and lateral directions.

2 Resonant frequencies of a bicycle rim

A bicycle rim without spokes will resonate at its natural frequencies when struck. These resonant modes are within the audible range and can be easily recorded with a standard smartphone microphone. The modes are classified into radial bending modes (rim moves entirely within its plane) and lateral-torsional modes (rim moves out of its plane). Although both types will be present in an experimental spectrum, they can be preferentially excited by striking the rim at different angles, much like how a percussionist can control the timbre of a gong or drum.

The natural frequencies of the radial bending modes depend on the rim properties as follows [14]:

$$f_n^{rad} = \frac{n(n^2 - 1)}{\sqrt{n^2 + 1}} \sqrt{\frac{EI_{11}}{2\pi R^3 M}} \quad (1)$$

where f_n^{rad} is the n th harmonic frequency, E is the Young's modulus, I_{11} is the second moment of area for in-plane bending, R is the radius of the rim at the centroid, and M is the total mass of the rim. The first mode $n = 1$ corresponds to a rigid-body motion with zero frequency. The fundamental vibration mode is $n = 2$. Having measured M and R and identified several modes from the frequency spectrum, the in-plane bending stiffness EI_{11} can be determined by solving Eqn. 1 and averaging the result from several different modes.

If warping is neglected, the frequencies of the lateral-torsional modes depend on the rim properties as follows [14]:

$$f_n^{lat} = \frac{n(n^2 - 1)}{\sqrt{\mu n^2 + 1}} \sqrt{\frac{GJ}{2\pi R^3 M}} \quad (2)$$

where $\mu = GJ/EI_{22}$, G is the shear modulus, J is the torsion constant, and I_{22} is the second moment of area for out-of-plane bending. Unlike Eqn. 1, Eqn. 2 depends on two independent stiffness parameters μ and GJ which must be determined simultaneously.

3 Experimental procedure

3.1 Acoustic Test

The impulse responses of seven aluminum rims of unknown properties were obtained by the following procedure: the rim was suspended by a string from the valve stem hole and struck with a screwdriver handle wrapped in rubber. The rim was struck first on the inside circumference and then on the sidewall at a point between two spoke holes approximately 10° from the

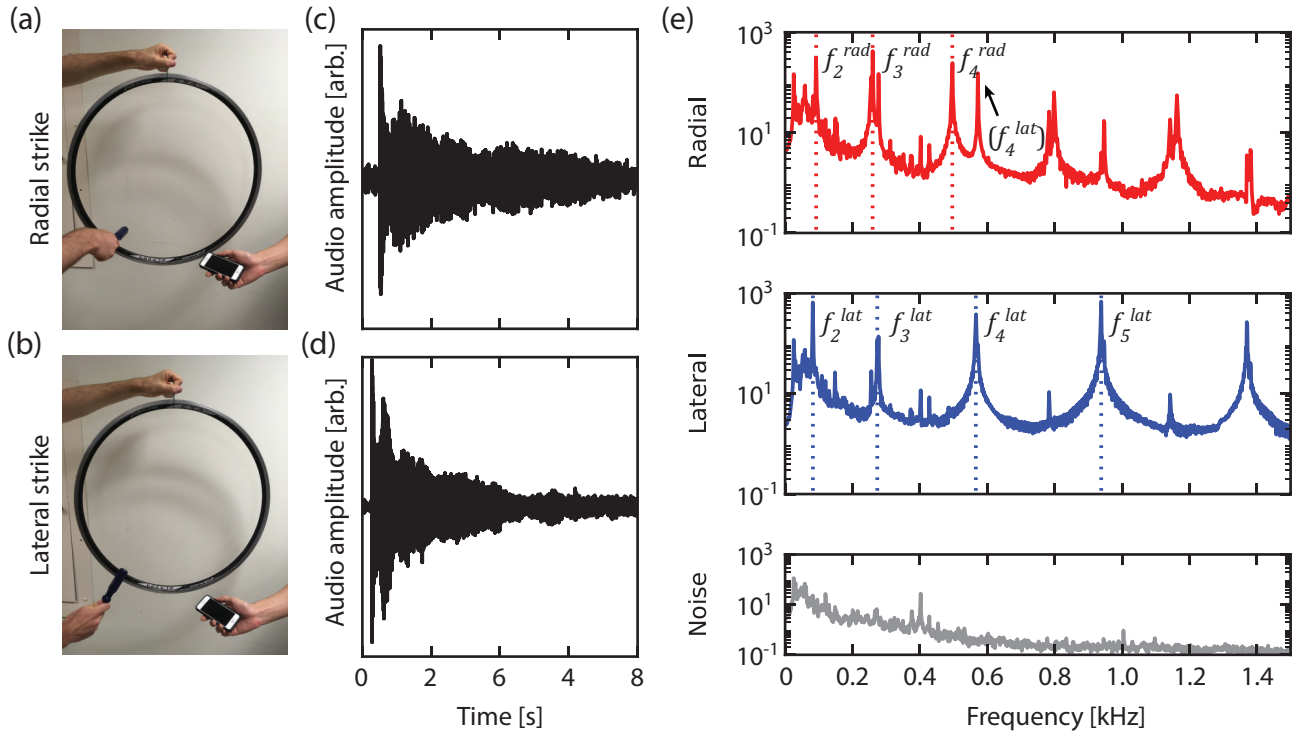


Fig. 1 (a)-(b) Experimental setup for radial and lateral strike test. (c)-(d) Time-domain signals for radial and lateral strike test. (e) Fourier spectrum for radial strike (top), lateral strike (middle), and background noise (bottom).

Table 1 Properties of the rims in this study.

Rim	Type ^a	R [mm]	M [g]
Alex ALX295	DDW	305	480
DT Swiss R460	DDW	304	459
Sun Ringle CR18 20"	DW	217	380
Sun Ringle CR18 700c	DW	304	540
Alex Y2000 26"	SW	271	460
Alex Y2000 700c	SW	302	551
Alex X404 27"	SW	307	594

^aCross-section type: DDW=deep double-wall, DW=double-wall, SW=single-wall.

bottom of the wheel to excite as many modes as possible. Audio was recorded with the “Recorder+” app on an iPhone SE using the built-in microphone at a sampling rate of 44.1 kHz. The frequency spectrum was estimated by averaging eight spectra calculated using the Fast Fourier Transform with a bandwidth of 1.35 Hz. A noise spectrum was also obtained by recording several seconds of silence in the same room. The frequency response of the built-in microphone was measured in an anechoic chamber (see Online Resource 1).

The peaks with a signal-to-noise ratio greater than 10 were identified and classified as radial or lateral modes depending on their relative magnitude in the two spectra. The frequency of each peak was determined by fit-

ting a Lorentzian function in the neighborhood of the maximum value. The two peaks at 27 Hz and 60 Hz were present in the noise spectrum and therefore rejected.

3.2 Diametral compression

The rims were then loaded in diametral compression under displacement control in an Instron MTS. The valve hole was placed at 45° from the load point where the bending moment is minimized to reduce its effect on the measurement. Castiglione’s method gives the deflection of a ring subjected to radial point loads [15]:

$$\delta = \frac{PR^3}{4EI_{11}} \left(\pi - \frac{8}{\pi} \right) \quad (3)$$

3.3 Four-point bending test

The lateral stiffness of each bicycle rim was also measured using a four-point bending test. The rim was supported at 3- and 9-o’clock by cylindrical rods and constrained against a rigid bracket on the top surface of the rim at 12-o’clock. The rim was then loaded by hanging a weight from the spoke hole (or valve hole) at 6-o’clock.

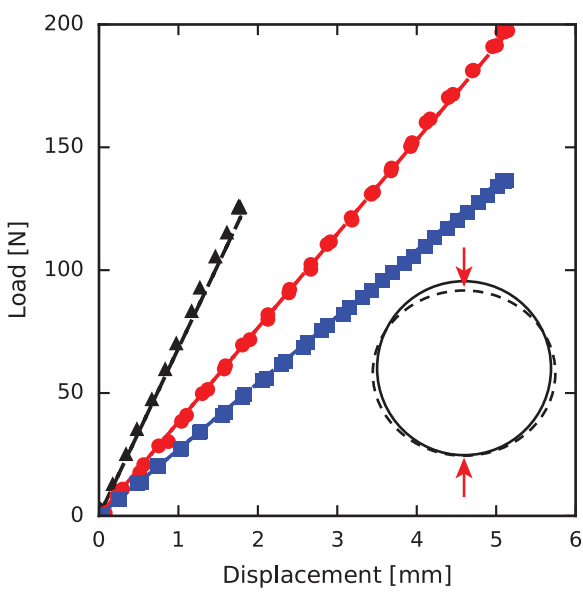


Fig. 2 Selected radial load-displacement curves under diametral compression. Black triangles = Alex ALX295, red circles = Alex Y2000 26", blue squares = Sun CR18 700c.



Fig. 3 Four-point bending test. A small mirror resting on the rim at 9-o'clock reflects the laser spot onto a grid (to the right, not shown). The un-balanced configuration effectively doubles the lateral displacement at the load point and increases sensitivity.

The vertical deflection at 6-o'clock was measured using a dial indicator and the rotation of the cross-section at 9-o'clock was measured by an optical lever with a diode laser.

If warping is neglected and only the strain energy due to lateral bending and uniform torsion are considered, Castigliano's method yields the displacement u_l at the load point and the rotation of the cross-section

ϕ_s at the left support (see Online Resource 1):

$$u_l = -\left(\frac{PR^3}{2GJ}\right)[(2(3-\pi) + \mu(2-\pi)] \quad (4)$$

$$\phi_s = -\left(\frac{PR^3}{8GJ}\right)(1+\mu)(2-\pi)$$

By simultaneously measuring the deflection and rotation, GJ and μ can be determined from a single test.

4 Results and discussion

4.1 Radial stiffness

After identifying the first several mode frequencies in each spectrum, $\sqrt{EI_{11}/2\pi R^3 M}$ was estimated from the fundamental ($n = 2$) mode. With knowledge of R and M , the radial bending stiffness was determined from Eqn. 1.

The results for the radial stiffness EI_{11} are shown in Fig. 4. The error estimates are made on the assumption that the mass and radius are both known to within 1%. The uncertainty in the frequency is the greater of either the estimated parameter variance from the Lorentzian fit, or the frequency resolution of the spectral average. Multiple modes may be averaged together to estimate EI_{11} , however the deviation from Eqn. 1 grows steadily larger with higher mode number due to the fact that shorter wavelengths interact with spoke holes and other inhomogeneities.

4.2 Lateral-torsional stiffness

Lateral bending and torsion are coupled in out-of-plane deformation modes of circular beams. Therefore, information from multiple modes must be used to calculate GJ and μ . Taking the ratio of two lateral-torsional frequencies and solving for μ in Eqn. 2 gives

$$\mu = \frac{16 - (f_3^{lat}/f_2^{lat})^2}{9(f_3^{lat}/f_2^{lat})^2 - 64} \quad (5)$$

After calculating μ , GJ can be calculated from Eqn. 2 by setting $n = 2$:

$$GJ = \left(\frac{4\mu + 1}{18}\right)\pi R^3 M (f_2^{lat})^2 \quad (6)$$

Qualitatively, GJ scales the magnitude of the frequencies and μ scales the spacing between modes. However, the situation is further complicated by the fact that the cross-section of the rim does not remain perfectly planar. This additional warping deformation introduces a length scale into the torsional stiffness which depends on the rim radius and mode number. In this

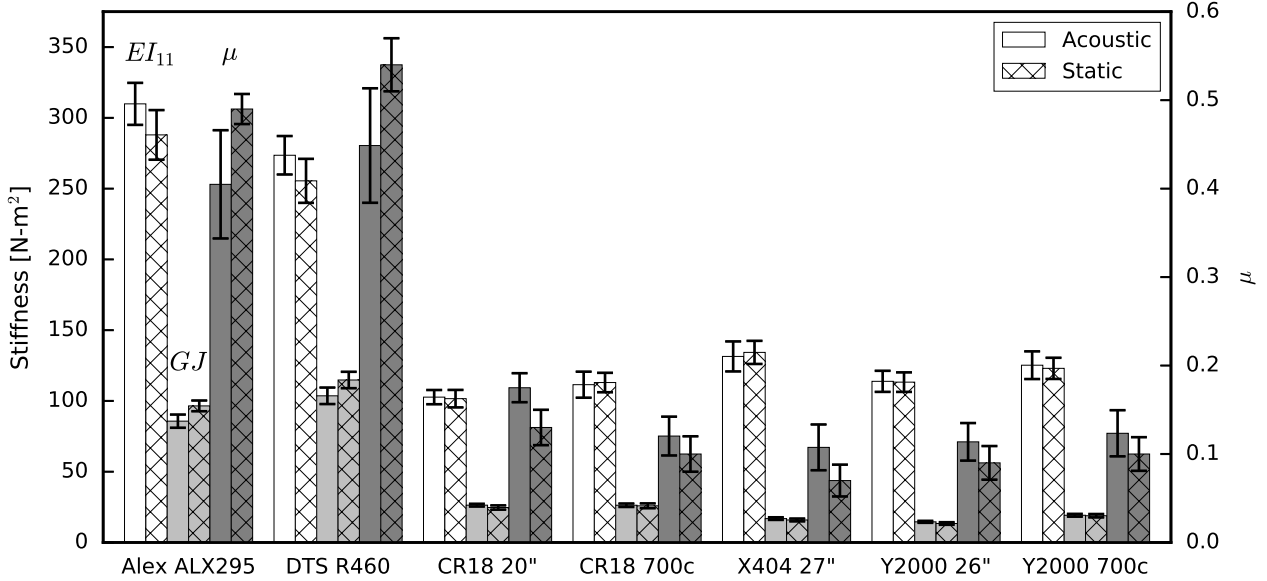


Fig. 4 Comparison of stiffness parameters calculated from the acoustic test vs. quasistatic load-displacement tests. For EI_{11} and GJ , refer to the left scale. For μ , refer to the right scale.

case the effective torsional response involves both GJ and EI_w , where I_w is the warping constant.

Results from the acoustic test and four-point bending test are shown Fig. 4. The value for μ is first calculated using Eqn. 5 and then GJ is determined from Eqn. 2 using the frequency of the $n = 2$ lateral-torsional mode. We choose to fit GJ because it is generally smaller than EI_{22} and therefore dominates the total flexibility.

The error estimates in Fig. 4 are made on the same assumptions as for EI_{11} . Due to the non-linearity of Eqn. 5, error estimates for μ are calculated using the Monte-Carlo method (see Online Resource 1). The lateral bending stiffness and torsion stiffness are geometrically coupled in lateral deformations. The total lateral-torsional stiffness depends on EI_{22} and GJ as though they were springs connected in series. The smaller stiffness dominates the overall stiffness of series-connected springs. Therefore GJ (generally smaller than EI_{22}) can be determined with much higher precision than EI_{22} or μ . Even a small uncertainty on f_3^{lat}/f_2^{lat} results in a large estimated uncertainty on μ and EI_{22} , but not GJ .

4.3 Lateral-torsional mode stiffness

An acoustic test is sufficient to calculate GJ to within 11% of the results from the four-point bending test. However, both models assume that warping is negligible. In fact, the acoustic test may be even more accurate than the four-point bending test because it di-

rectly measures the mode stiffness of the rim, which includes bending, pure torsion, and warping. In order to account for warping, we derive the frequency equation for lateral-torsional vibrations with an additional term for the warping resistance:

The differential equations of dynamic equilibrium, including warping but neglecting the rotary inertia of the rim cross-section, are

$$\frac{EI_{22}}{R^4} \left(\frac{d^4 u}{d\theta^4} - R \frac{d^2 \phi}{d\theta^2} \right) + \frac{EI_w}{R^6} \left(\frac{d^4 u}{d\theta^4} + R \frac{d^4 \phi}{d\theta^4} \right) - \frac{GJ}{R^4} \left(\frac{d^2 u}{d\theta^2} + R \frac{d^2 \phi}{d\theta^2} \right) + \left(\frac{M}{2\pi R} \right) \frac{d^2 u}{dt^2} = 0 \quad (7)$$

$$\frac{EI_{22}}{R^3} \left(\frac{d^2 u}{d\theta^2} - R \phi \right) - \frac{EI_w}{R^5} \left(\frac{d^4 u}{d\theta^4} + R \frac{d^4 \phi}{d\theta^4} \right) + \frac{GJ}{R^3} \left(\frac{d^2 u}{d\theta^2} + R \frac{d^2 \phi}{d\theta^2} \right) = 0 \quad (8)$$

We are seeking free vibrations of the form

$$u(\theta, t) = u_n e^{in\theta} e^{i\omega t} \quad (9)$$

$$\phi(\theta, t) = \phi_n e^{in\theta} e^{i\omega t}$$

Inserting Eqns. 9 into Eqns. 7 and 8 yields a linear system of the form $\mathbf{A} \cdot [u_n, \phi_n]^T = \mathbf{0}$. Non-trivial solutions exist when the determinant of the matrix \mathbf{A} vanishes. Using this condition to solve for the angular frequency ω yields the frequency equation:

$$\omega^2 = \frac{2\pi n^2 (n^2 - 1)^2 EI_{22} (GJ + \frac{EI_w}{R^2} n^2)}{MR^3 (EI_{22} + GJ n^2 + \frac{EI_w}{R^2} n^4)} \quad (10)$$

Exploiting the analogy with the simple harmonic oscillator, for which $\omega^2 = K/M$, allows us to calculate an effective rim stiffness of the n th mode:

$$K_{rim,n} = 2 \left(\frac{R^3}{\pi n^2 (n^2 - 1)^2 (GJ + \frac{EI_w}{R^2} n^2)} + \frac{R^3}{\pi (n^2 - 1)^2 EI_{22}} \right)^{-1} \quad (11)$$

Comparing Eqn. 11 with Eqns. 34 and 35 in reference [8], it's clear that the effective stiffness is twice the series combination of the rim bending stiffness and torsion stiffness. Even if EI_{22} and GJ cannot be reliably determined independently, the series combination can be directly determined from the relation $f_n^{lat} = (2\pi)^{-1} \sqrt{K_{rim,n}/M}$.

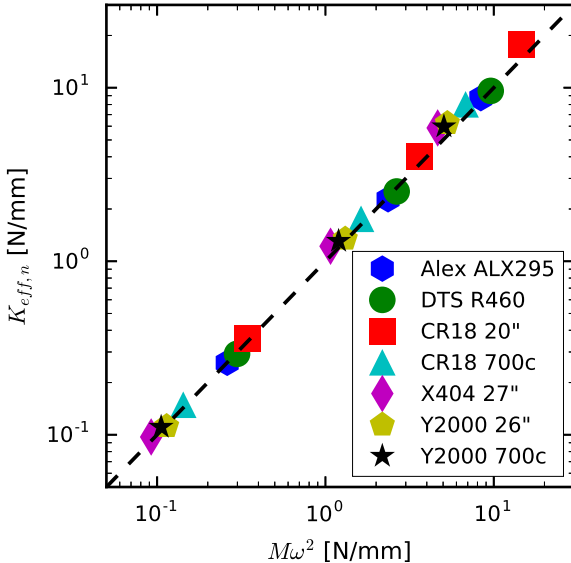


Fig. 5 Comparison of mode stiffness from the acoustic test (x-axis) and the mode stiffness calculated from Eqn. 11 and the stiffness parameters determined from the four-point bending test. The error increases at higher mode numbers, likely due to the length-scale dependence of the warping stiffness.

4.4 Stiffness of a complete wheel

The deformed shape of a wheel with spokes can be written as a superposition of modes of the form $u = u_n \cos(n\theta)$. The lateral stiffness can be decomposed into a series of equivalent springs for each mode [8]. The total lateral stiffness of the wheel is

$$\frac{1}{K_{lat}} = \frac{3}{2K_{spokes}} + \sum_{n=2}^{\infty} \frac{1}{\frac{1}{2}K_{rim,n} + K_{spokes}} \quad (12)$$

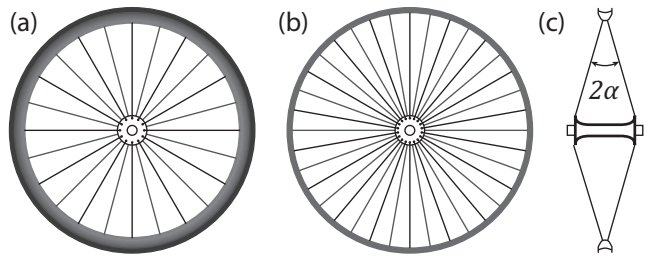


Fig. 6 Example wheels for stiffness calculation: (a) Modern racing bike wheel. (b) Vintage road bike wheel. (c) Side-view showing spoke angle.

where

$$K_{spokes} = \frac{n_s k_s}{2} \sin^2 \alpha \quad (13)$$

where n_s is the number of spokes, k_s is the axial spring constant of a single spoke, and α is the angle between the spoke and the plane of the wheel¹ as shown in Fig. 6. When calculating the wheel stiffness (with spokes), the first two static modes, $n = 0$ and $n = 1$, represent rigid-body motions of the rim, so only the spoke stiffness is involved.

Table 2 Example wheel properties.

Wheel	GJ	EI_{22}	K_{spokes} [N/mm]	K_{lat} [N/mm]
Modern	94.0	206	304	121
Vintage	16.8	158	461	147

Bicycle wheels are often marketed on their stiffness, which is prized for its presumed benefits to performance and durability. However, as modern rims have become stiffer, wheel manufacturers have followed a trend towards fewer spokes as a way to save weight, reduce drag, and cut costs. How might a modern wheel compare with a typical road wheel from the 1970's?

As an example calculation, let us consider two hypothetical front wheels with the same hub width (60 mm): (a) a modern racing bicycle wheel constructed from the Alex ALX295 rim (a modern deep double-wall rim) with 24 lightweight 1.7/2.0 mm spokes, and (b) a vintage road bicycle wheel constructed from the X404-27" rim (a shallow single-wall rim) with 36 2 mm spokes. Using the mode stiffnesses measured from our acoustic test together with Eqn. 12, wheel (a) has a theoretical lateral stiffness of 121 N/mm while wheel (b) has a theoretical stiffness of 147 N/mm. The stiffer (and heavier) spokes in wheel (b) make up for its relatively

¹ Equation 13 is strictly valid for symmetric radially-spoked wheels, but gives a good approximation for other cases. See reference [8].

flexible rim. Since the mode stiffnesses in Eqn. 12 add in series, even a wheel with an infinitely stiff rim will reach a maximum stiffness defined by its spoke system.

5 Conclusion

Acoustic EMA gives estimates of EI_{11} and GJ which agree to within 8% and 11% respectively compared to the results from static deflection tests for the seven rims tested in this study. Together with the geometry of the wheel and the axial stiffness of the spokes, these properties can be used to make quantitative predictions about wheel stiffness, maximum tension, and truing response. Furthermore, the acoustic measurement can be performed with a smartphone, tape measure, and scale. The technique is suitable for automation and could be packaged into a smartphone app for wheelbuilders or bicycle designers.

The acoustic test also gives a direct measurement of the lateral-torsional mode stiffnesses. When added together using the series-springs rule, the rim mode stiffnesses in parallel with the spoke stiffness gives the wheel lateral stiffness [8]. In practice, only the first 3 rim modes need to be measured because the mode stiffness increases dramatically with mode number.

Acknowledgements This material is based upon work supported by the National Science Foundation Graduate Research Fellowship Program under Grant No. DGE-1324585. Any opinions, findings, and conclusions or recommendations expressed in this material are those of the authors and do not necessarily reflect the views of the National Science Foundation. This research was also supported by a Grant-In-Aid of Research from Sigma Xi.

We would like to thank Dr. Joel Fenner for his help performing the diametral compression tests, and Professor Jonathan Siegel and the Department of Communication Sciences and Disorders at Northwestern for the use of their anechoic chamber. We are also grateful to Professor Jim Papadopoulos for many enlightening discussions on bicycle wheel mechanics.

This is a pre-print of an article published in Journal of Nondestructive Evaluation. The final authenticated version is available online at: <https://doi.org/10.1007/s10921-018-0471-7>.

References

1. Feng, M., Fukuda, Y., Mizuta, M., Ozer, E.: Citizen sensors for SHM: Use of accelerometer data from smartphones. *Sensors (Switzerland)* **15**(2), 2980–2998 (2015). DOI 10.3390/s150202980
2. Morgenthal, G., Höpfner, H.: The application of smartphones to measuring transient structural displacements. *J. Civ. Struct. Heal. Monit.* **2**(3-4), 149–161 (2012). DOI 10.1007/s13349-012-0025-0
3. Kong, Q., Allen, R.M., Schreier, L., Kwon, Y.W.: MyShake: A smartphone seismic network for earthquake early warning and beyond. *Sci. Adv.* **2**(2), e1501,055 (2016). DOI 10.1126/sciadv.1501055
4. Grebenik, J., Zhang, Y., Bingham, C., Srivastava, S.: Roller element bearing acoustic fault detection using smartphone and consumer microphones comparing with vibration techniques. In: 17th Int. Conf. Mechatronics - Mechatronika, 1, pp. 1–7 (2016)
5. Pepelko, D.: Spoke Tension Gauge (2016). Available from iTunes App Store
6. Pippard, A.S., Francis, W.: On a Theoretical and Experimental Investigation of the Stresses in a Radially Spoked Wire Wheel under Loads applied to the Rim. *Philos. Mag.* **11**(69), 233–285 (1931). DOI 10.1080/14786443109461681
7. Papadopoulos, J.M.: Method for Trueing Spoked Wheels (1992). US Patent 5103414
8. Ford, M., Papadopoulos, J.M., Balogun, O.: Buckling of the bicycle wheel. In: Proc. 2016 Bicycl. Mot. Dyn. Conf. (2016). DOI 10.6084/m9.figshare.3856134
9. Gavin, H.P.: Bicycle-Wheel Spoke Patterns and Spoke Fatigue. *J. Eng. Mech.* **122**(8), 736–742 (1996). DOI 10.1061/(ASCE)0733-9399(1996)122:8(736)
10. Pippard, A.S., Francis, W.: The Stresses in a Wire Wheel under Side Loads on the Rim. *Philos. Mag.* **14**(91), 436–445 (1932). DOI 10.1080/14786443209462081
11. Burgoyne, C., Dilmaghalian, R.: Bicycle wheel as prestressed structure. *J. Eng. Mech.* **119**(3), 439–455 (1993). DOI 10.1061/(ASCE)0733-9399(1993)119:3(439)
12. Ewins, D.: Modal testing: theory and practice. Wiley, New York, NY (1984)
13. Salawu, O.: Detection of structural damage through changes in frequency: a review. *Eng. Struct.* **19**(9), 718–723 (1997). DOI 10.1016/S0141-0296(96)00149-6
14. Timoshenko, S.P., Young, D.: *Vibration Problems in Engineering*, 3rd ed. edn. D. Van Nostrand Company, New York, NY (1955)
15. Timoshenko, S.P., Gere, J.M.: *Theory of Elastic Stability*, 2nd edn. McGraw-Hill, New York, NY (1961)